

The effects of surface mass flux on the instability of the BEK system of rotating boundary-layer flows

R.J. Lingwood^{a,b}, S.J. Garrett^{c,*}

^a Linné Flow Centre, KTH Mechanics, Royal Institute of Technology, SE-100 44, Stockholm, Sweden

^b University of Cambridge, Cambridge, CB23 8AQ, UK

^c Department of Mathematics, University of Leicester, University Road, Leicester, LE1 7RH, UK

ARTICLE INFO

Article history:

Received 23 September 2010

Received in revised form

13 December 2010

Accepted 3 February 2011

Available online 15 February 2011

Keywords:

Boundary layer

BEK system

Convective instability

Absolute instability

ABSTRACT

We consider the effect of mass flux through the lower boundary of the general class of rotating BEK boundary-layer flows. This class includes the Bödewadt, Ekman and von Kármán flows as particular cases. A theoretical study is presented which considers the onset of convective instability modes (both stationary and travelling relative to the rotating system) and local absolute instability. Suction is found to be universally stabilising in terms of both the delayed onset and reduced amplification rates of both instability types. Furthermore, the radial span of convective instability preceding the onset of local absolute instability is extended with increased suction. Slowly travelling modes are predicted to be more dangerous than stationary modes within the convectively unstable region of each flow. Such modes are expected to be selected over highly polished lower disks. Extensive theoretical data is presented for future comparison to experiment.

© 2011 Elsevier Masson SAS. All rights reserved.

1. Introduction

This paper details the stability properties of the family of boundary-layer flows caused by a differential rotation rate between a lower disk and an incompressible fluid in rigid-body rotation above. Particular cases are the Bödewadt, Ekman and von Kármán boundary layers, hence this family is referred to as the BEK system. The Bödewadt layer arises when the lower disk is stationary and the fluid rotates; the Ekman layer has the disk and fluid rotating at approximately the same rate; and the von Kármán layer has the disk rotating in otherwise still fluid. In each case the lower disk is permeable, allowing enforced mass flux (injection or suction) in the normal direction.

There has been considerable interest in the stability characteristics of three-dimensional rotating boundary-layer flows since Gregory et al. [1] first studied the stability properties of the von Kármán boundary layer in the mid 1950s. This benchmark rotating system still remains of interest today due to its similarity to the practically significant flow over a swept wing. However, a natural extension to this model flow is the introduction of an additional rotating disk in the far field above, this leads to the BEK class of

flows with the differential rotation rate as a key system parameter. In addition to having a theoretical interest, this broad class of flows can occur in turbo-machinery and rotor-stator devices such as mixers. Their stability characteristics therefore have practical importance. Furthermore, the stability characteristics of the Ekman layer may have applications for geophysical flows as discussed by Lingwood [2] and the references contained therein. In this paper we are motivated by turbo-machinery applications where laminar flow should be maintained as far as possible and suction is a potential stabilising mechanism. However, we acknowledge that the encouragement of turbulence may be beneficial for heat diffusion and mixing problems, and we also present mass-injection results.

The similarities in the stability characteristics of all flows within the BEK class are well established. See, for example, the experimental studies of [3,4] for the Ekman layer; [5–7] for the von Kármán flow; and [8–12] for the Bödewadt layer. In all systems, spiral waves associated with the convective instability of the flow and rotating with the lower disk have been observed in regions outside the turbulent regime; see for example [1,4,13,2]. The systems are all convectively unstable within certain regions to disturbances stationary in the frame rotating with the disk. These disturbances are excited by roughnesses on the disk surface and, because these roughnesses are fixed in time in the rotating frame, the stationary disturbances are consistently excited and reinforced such that they are evident in flow-visualisation experiments and in quantitative experiments, e.g. using hot-wire anemometry, where measurements tend to be ensemble averaged over many

* Corresponding author. Tel.: +44 0 116 252 3899.

E-mail addresses: rjl1001@cam.ac.uk (R.J. Lingwood), s.garrett@mcs.le.ac.uk, sjg50@le.ac.uk (S.J. Garrett).

URL: <http://www.tinyurl.com/SJGarrett> (S.J. Garrett).

periods of rotations to improve the signal-to-noise ratio. The systems are also all convectively unstable within certain regions to disturbances that are not stationary in the frame rotating with the disk, i.e., travelling disturbances. However, travelling disturbances, which are excited by, for example, freestream turbulence, have received less attention because unless they are intentionally and repeatably excited (as in Lingwood [6]) flow-visualisation and ensemble-averaging techniques average the signals away. Furthermore, it is known that the class of flows is locally absolutely unstable [2,14] and it is travelling modes that play a particular role in this instability mechanism. Although the determination of a local absolute instability requires the so-called parallel-flow approximation to be made (although the boundary-layer flows are physically parallel this terminology is used to describe the approximation of ignoring variations in Reynolds number with radius needed to render the linearised perturbation equations separable; see [15–18]), it is clear that the observed repeatable onset of transition to turbulence of many of these flows is due to a related global physical phenomenon. The exact mechanism involved remains an active research area (see [19], for example) and the study of local absolute instability continues to be of significance.

Suction typically acts as a stabilising mechanism in boundary-layer flows. For example, Gregory and Walker [20] discuss how the introduction of suction extends the laminar-flow region over a swept wing by reducing the thickness of the boundary layer and the magnitude of crossflow velocity. As before, insight into swept-wing flow arose from studies of the von Kármán boundary layer (see [21,22]) and work continued on this model flow with suction using numerical and asymptotic approaches (see [23–26], for example). The literature shows that suction has a stabilising effect on the von Kármán flow which results in an increase in critical Reynolds numbers, a narrowing in the range of unstable parameters and a decrease in the amplification rates of unstable convective modes. In addition, Lingwood [27] demonstrates that suction has a stabilising effect on local absolute instability. Furthermore, the recent paper of Culverhouse et al. uses numerical and asymptotic techniques to consider the stabilising effects of suction on convective modes within the Bödewadt layer. All studies have shown injection to have the converse effect by destabilising the boundary layer to both instability types.

In this paper we extend both Lingwood and Culverhouse et al. by considering the effects of suction and injection on the stability characteristics of the entire class of BEK flows. In Section 2 the problem is formulated and steady laminar-flow profiles are calculated. In Section 3 convective instability modes are considered and neutral curves and critical Reynolds numbers are presented for a variety of flow parameters. In Section 4 local absolute instability is considered and our conclusions are drawn in Section 5. We are unable to obtain experimental data for comparison for flows other than the von Kármán and Bödewadt cases previously considered by Lingwood and Culverhouse et al., we therefore present detailed predictions of measurable quantities in the Appendix. It is hoped that these can be referred to when experimental data becomes available.

2. Formulation

2.1. The steady flow

The formulation of the problem for the general BEK system with mass flux is very closely related to that presented by Lingwood [2] and is summarised here for completeness. The radius of the lower disk and the extent of the fluid above are assumed to be infinite, and the disk and fluid rotate about the same vertical axis with angular velocities Ω_D^* and Ω_F^* , respectively. The Bödewadt layer

has $\Omega_D^* = 0$ and $\Omega_F^* \neq 0$; the Ekman layer has $\Omega_D^* \approx \Omega_F^*$; and the von Kármán layer has $\Omega_D^* \neq 0$ and $\Omega_F^* = 0$. Between these particular cases are flows in which both the disk and fluid rotate with different angular velocities. Although the model is valid for counter- and co-rotating systems, only co-rotating systems will be studied here.

The dimensional Navier–Stokes equations for the axisymmetric mean flow are formulated in cylindrical-polar coordinates r^* , θ and z^* , in a frame rotating at Ω_D^* , i.e., with the lower disk. These are stated by Lingwood [2] as Eqs. (3.1)–(3.4). The mean radial, azimuthal and axial velocities are given by an extension of the exact similarity solution for the von Kármán flow [28], as is the pressure, such that the scaled variables are respectively given by

$$\begin{aligned} U(z) &= \frac{U^*}{r^* \Omega^* Ro}, & V(z) &= \frac{V^*}{r^* \Omega^* Ro}, \\ W(z) &= \frac{W^*}{l^* \Omega^* Ro}, & P(r, z) &= \frac{P^*}{\rho^* l^{*2} \Omega^{*2} Ro^2}. \end{aligned} \quad (1)$$

Here, r and z are the dimensionless forms of r^* and z^* , scaled on a measure of the boundary-layer thickness $l^* = \sqrt{v^*/\Omega^*}$. Furthermore, Ro is the Rossby number and Ω^* is the system rotation rate respectively defined as

$$Ro = \frac{\Omega_F^* - \Omega_D^*}{\Omega^*}, \quad (2)$$

$$\begin{aligned} \Omega^* &= \frac{\Omega_F^*}{2 - Ro} + \frac{\Omega_D^*}{2 - Ro} \\ &= \frac{\Omega_F^* + \Omega_D^*}{4} + \left(\left(\frac{\Omega_F^* + \Omega_D^*}{4} \right)^2 + \frac{(\Omega_F^* - \Omega_D^*)^2}{2} \right)^{1/2}. \end{aligned} \quad (3)$$

In addition, we define the Coriolis parameter $Co = 2\Omega_D^*/\Omega^* = 2 - Ro - Ro^2$. In terms of these parameters, the three particular cases within the family are classified as:

Bödewadt layer: $Ro = 1$ $Co = 0$ $\Omega^* = \Omega_F^*$

Ekman layer: $Ro = 0$ $Co = 2$ $\Omega^* = \Omega_F^* = \Omega_D^*$

von Kármán layer: $Ro = -1$ $Co = 2$ $\Omega^* = \Omega_D^*$.

As discussed by Lingwood [2], this formulation leads to non-dimensional ordinary differential equations (ODEs) for the mean flow¹

$$2U + W' = 0, \quad (4)$$

$$Ro(U^2 + WU' - (V^2 - 1)) - Co(V - 1) - U'' = 0 \quad (5)$$

$$Ro(2UV + WV') + CoU - V'' = 0 \quad (6)$$

$$Ro(WW' + P') - W'' = 0, \quad (7)$$

where a prime denotes differentiation with respect to z . These are subject to the boundary conditions

$$U(0) = V(0) = W(0) + a = 0, \quad (8)$$

$$U(z \rightarrow \infty) = 0, \quad V(z \rightarrow \infty) = 1, \quad (9)$$

which represent non-slip and non-zero normal mass flux through the lower disk surface (characterised by parameter a), and the rotating far-field flow, respectively. We note that the sign of the dimensional flow components depend on the sign of Ro and this has implications for the interpretation of a : for $Ro > 0$, positive a is interpreted as suction, and for $Ro < 0$, positive a is interpreted as injection. For ease of presentation we define a suction parameter

$$a_s = \begin{cases} a, & \text{if } Ro \geq 0, \\ -a, & \text{if } Ro < 0, \end{cases}$$

¹ We note a typographical error in [2]: the variable H in Eqs. (3.11)–(3.14) should read W .

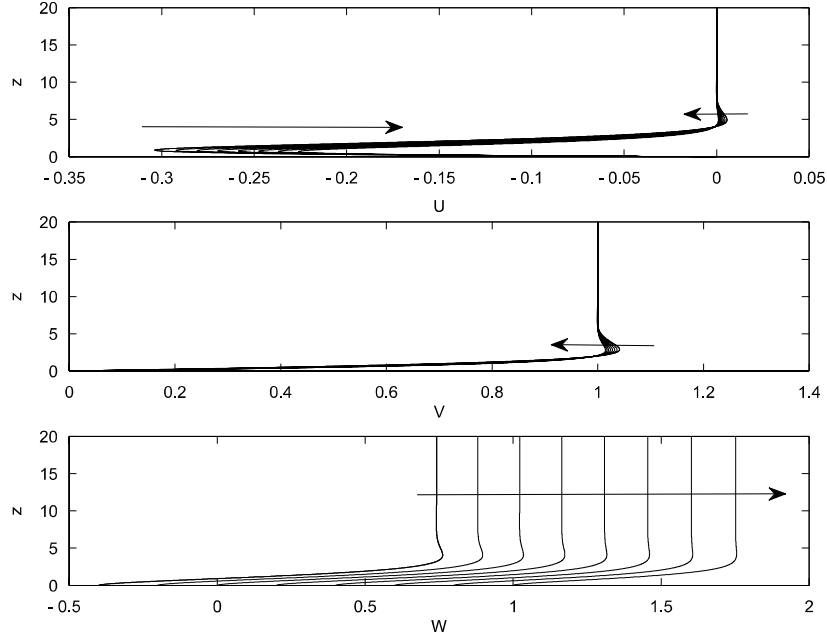


Fig. 1. Mean flow components for $Ro = -0.5$ at $a_s = -0.4, -0.2, \dots, 1$. Arrows indicate increasing suction. Note that the physical flows are the negative of these.

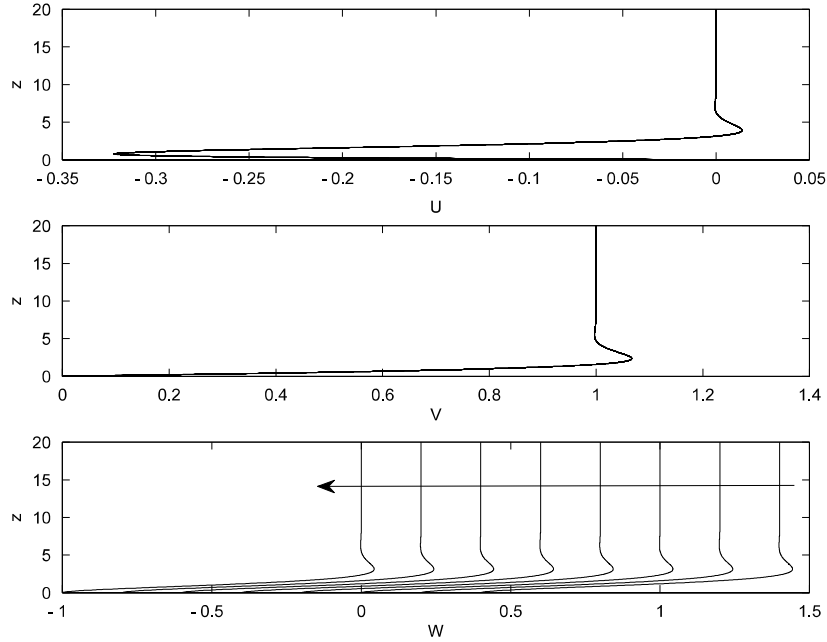


Fig. 2. Mean flow components for $Ro = 0$ at $a_s = -0.4, -0.2, \dots, 1$. Arrows indicate increasing suction.

such that positive a_s indicates suction for all Ro . As discussed in Section 1, it is the stabilisation of the boundary layers via suction that is of primary interest and so we consider a larger range of mass-flux parameter corresponding to suction. In particular this study will be limited to $-0.4 \leq a_s \leq 1$, although this range could be arbitrarily extended within this formulation.

Culverhouse et al. [29] notes that the mean-flow components for the Bödewadt system ($Ro = 1$) are oscillatory through the boundary layer. This is also true for general Ro , although to a lesser extent as Ro is reduced from unity. It is therefore necessary to capture analytically the behaviour of the flow at the edge of boundary layer when solving the equations and integrate downwards. We follow the method described by van de Vooren et al. [30] and Culverhouse et al. to obtain the far-field conditions at a suitably high value of z (taken to be $z = 28$) and integrate downwards using a

fourth-order Runge–Kutta method. The resulting flow profiles for $Ro = -1$ are given by Lingwood [2] (Fig. 1), and for $Ro = 1$ by Culverhouse et al. (Fig. 1); we give profiles for $Ro = -0.5, 0$ and 0.5 as Figs. 1–3 respectively, each for $a_s = -0.4, -0.2, \dots, 1$.

Fig. 2 demonstrates that the radial and azimuthal flow components of the Ekman flow ($Ro = 0$) are independent of the mass-flux parameter. Mathematically, this reflects the decoupling of Eqs. (5) and (6) from (4) and (7), meaning that the U -and V -flow components are determined without regard to the axial-flow boundary conditions. Physically it is suggested that this is due to zero torsion between the upper and lower rotating flows, leading to a decoupling of the through flow in the axial direction. The implications of this for the stability of the Ekman layer are discussed in Section 3.1.

For the von Kármán layer ($Ro = -1$), Lingwood [2] reports that suction acts to increase the magnitude of axial flow in the

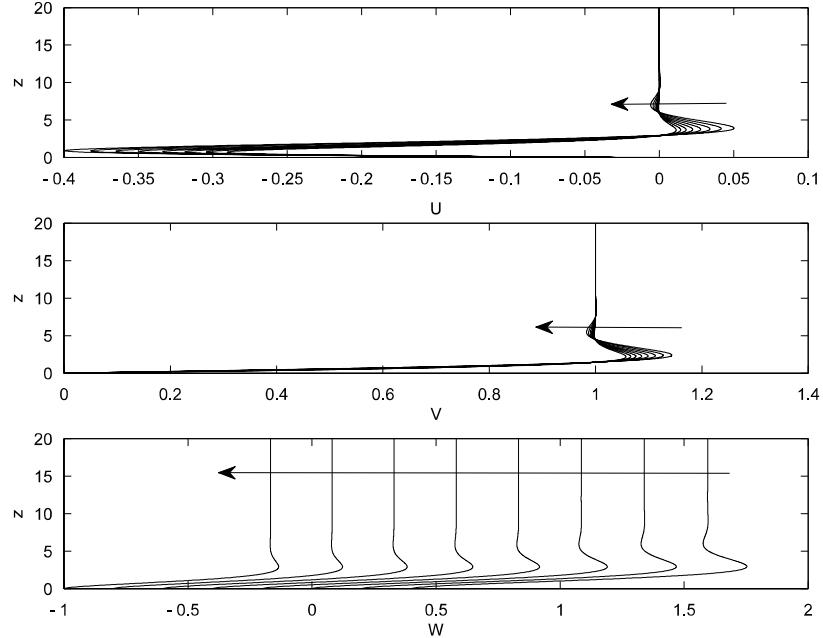


Fig. 3. Mean flow components for $\text{Ro} = 0.5$ at $a_s = -0.4, -0.2, \dots, 1$. Arrows indicate increasing suction.

far field; this is found here for all $\text{Ro} < 0$. In contrast, suction is found to reduce the magnitude of axial flow in the far field for $\text{Ro} \geq 0$. For all $\text{Ro} \neq 0$ the magnitude of oscillations in the radial and azimuthal components are reduced with increased suction, this is consistent with the findings of Lingwood and Culverhouse et al. Where appropriate, comparisons of the numerical values of $U'(0)$ and $V'(0)$ and $W(z \rightarrow \infty)$ have been made with existing calculations by Lingwood [2], MacKerrell [31] and Culverhouse et al., and excellent agreement is found in all cases.

For $\text{Ro} < 0$ the dimensional flow is the negative of the scaled version shown in Fig. 1 and the radial mean flow is directed predominantly outwards. Any convective modes would therefore also propagate outwards. In contrast, for $\text{Ro} \geq 0$ the radial mean flow is directed predominantly inwards and any convective modes would propagate in this direction. This has implications for the interpretation of the stability results presented in Sections 3 and 4, and these are discussed in Section 5.

2.2. The perturbation equations

Local linear stability analyses will be conducted at location r_a^* on the lower disk by imposing infinitesimally small disturbances on the mean flow. It is necessary to use a local Reynolds number

$$\text{Re} = \frac{r_a^* \Delta \Omega^* l^*}{\nu^*} = r_a \text{Ro}. \quad (10)$$

For negative Rossby number the Reynolds number is also negative, however this is a consequence of the formulation and all results will be presented in terms of positive Re for all Ro . We see that the Reynolds number can be interpreted as the non-dimensional location of the local analysis, and increasing Re corresponds to moving radially outwards from the axis of rotation (irrespective of the sign of the Rossby number). The perturbing velocities, pressure and time scales are non-dimensionalised on $r_a^* \Omega^* \text{Ro}$, $\rho^* r_a^{*2} \text{Ro}^2$ and $l^*/(r_a^* \Omega^* \text{Ro})$, respectively. These lead to instantaneous non-dimensional velocities and pressure given by

$$\begin{aligned} \bar{u}(r, \theta, z, t; \text{Ro}, a_s) \\ = \frac{r \text{Ro}}{\text{Re}} U(z; \text{Ro}, a_s) + u(r, \theta, z, t; \text{Re}, \text{Ro}, a_s), \end{aligned}$$

$$\begin{aligned} \bar{v}(r, \theta, z, t; \text{Ro}, a_s) \\ = \frac{r \text{Ro}}{\text{Re}} V(z; \text{Ro}, a_s) + v(r, \theta, z, t; \text{Re}, \text{Ro}, a_s), \\ \bar{w}(r, \theta, z, t; \text{Ro}, a_s) \\ = \frac{\text{Ro}}{\text{Re}} W(z; \text{Ro}, a_s) + w(r, \theta, z, t; \text{Re}, \text{Ro}, a_s), \\ \bar{p}(r, \theta, z, t; \text{Ro}, a_s) \\ = \frac{\text{Ro}^2}{\text{Re}^2} P(r, z; \text{Ro}, a_s) + p(r, \theta, z, t; \text{Re}, \text{Ro}, a_s), \end{aligned}$$

where u, v, w and p are small perturbing quantities.

The dimensionless Navier–Stokes equations in cylindrical-polar coordinates are linearised with respect to the perturbing quantities and we ignore variation in Reynolds number with radius. This approximation is often referred to as the parallel-flow approximation and is necessary here to make the linearised equations separable in r , θ and t . In practice this involves replacing the variable r that appears in the coefficients of the linearised perturbation equations with Re . However, note that this approximation is not necessary in the Ekman case. Terms at $O((\text{Ro}/\text{Re})^2)$ are neglected and the perturbation quantities are assumed to have the normal-mode form:

$$(u, v, w, p) = (\hat{u}, \hat{v}, \hat{w}, \hat{p})(z; \alpha, \beta, \omega; \text{Re}, \text{Ro}, a_s) e^{i(\alpha r + \beta \theta - \omega t)} + \text{c.c.}$$

Here the hat indicates a spectral representation of the perturbing quantities. The parameters α and $\beta = \beta \text{Re}/\text{Ro}$ are the radial and azimuthal wavenumbers, respectively. Furthermore, ω is the frequency of disturbances in the frame rotating at Ω_D^* . The formulation leads to ω taking the opposite sign to ω^* for negative Rossby number, however the results are presented with ω and ω^* having the same sign for all Ro . The spatio-temporal stability analyses presented later require that $\alpha = \alpha_r + i\alpha_i$ and $\omega = \omega_r + i\omega_i$, with β real and integer to enforce periodicity around the azimuth.

As discussed by Lingwood [2], we introduce the transformed variables

$$\begin{aligned} \phi_1 &= \bar{\alpha} \hat{u} + \beta \hat{v}, & \phi_2 &= \bar{\alpha} \hat{u}' + \beta \hat{v}' \\ \phi_3 &= \hat{w}, & \phi_4 &= \hat{p}, \\ \phi_5 &= \bar{\alpha} \hat{v} - \beta \hat{u}, & \phi_6 &= \bar{\alpha} \hat{v}' - \beta \hat{u}', \end{aligned}$$

Table 1

Critical Reynolds numbers Re at the onset of stationary type I lobes. Where appropriate the critical value at the onset of the stationary type II lobe is also shown, (*italics*).

Ro	$a_s = -0.4$	$a_s = -0.2$	$a_s = 0$	$a_s = 0.2$	$a_s = 0.4$	$a_s = 0.6$	$a_s = 0.8$	$a_s = 1.0$
-0.8	158.3	184.8	216.8	255.6 (398.9)	303.0 (444.6)	361.1 (497.7)	432.4 (562.1)	520.4 (641.7)
-0.6	138.0	155.0	174.4	196.5	221.8	250.7 (356.5)	283.7 (388.3)	321.6 (423.4)
-0.4	128.0	138.5	149.9	162.3	175.7	190.4	206.5	223.7
-0.2	121.8	126.7	132.0	137.4	143.1	149.0	155.1	161.6
0	116.3	116.3	116.3	116.3	116.3	116.3	116.3	116.3
0.2	92.4	96.5	100.9	105.4	110.1	115.1	120.2	125.6
0.4	69.9	76.9	85.0	93.0	102.2	112.2	123.2	135.1
0.6	48.5	57.0	66.9	78.4	91.7	106.9	124.5	144.6
0.8	28.7	37.0	47.6	61.1	77.6	98.0	123.0	153.3
1	13.9	19.2	27.4	40.5	58.9	70.5 (75.3)	117.1 (110.0)	(142.6)

where $\bar{\alpha} = \alpha - iRo/Re$, and write the perturbation equations as a set of six first-order ODEs.

$$\phi'_1 = \phi_2, \quad (11)$$

$$\phi'_2 = (\gamma^2 + iRe(\alpha U + \beta V - \omega) + RoU)\phi_1 + RoW\phi_2 + (\bar{\alpha}U' + \beta V')Re\phi_3 + i\gamma^2Re\phi_4 - (2RoV + Co)\phi_5, \quad (12)$$

$$\phi'_3 = -i\phi_1, \quad (13)$$

$$\phi'_4 = iRoW\phi_1/Re - i\phi_2/Re - (\gamma^2 + iRe(\alpha U + \beta V - \omega) + RoW')\phi_3/Re, \quad (14)$$

$$\phi'_5 = \phi_6, \quad (15)$$

$$\phi'_6 = (2RoV + Co)\phi_1 + (\bar{\alpha}V' - \beta U')Re\phi_3 + \beta Ro\phi_4 + (\gamma^2 + iRe(\alpha U + \beta V - \omega) + RoU)\phi_5 + RoW\phi_6, \quad (16)$$

where $\gamma^2 = \alpha^2 + \beta^2$ and $\bar{\gamma}^2 = \alpha\bar{\alpha} + \beta^2$. Lingwood [2] shows these equations to be consistent with the standard equations of stability theory when terms arising from streamline curvature and then viscosity are neglected.

In the following sections we solve the eigenvalue problem defined by (11)–(16), with the homogeneous boundary conditions

$$\begin{aligned} \phi_i &= 0, & \eta &= 0, \\ \phi_i &\rightarrow 0, & \eta &\rightarrow \infty, \end{aligned} \quad (17)$$

for $i = 1, 2, \dots, 6$. The resulting eigenvalue problem can be solved for certain combinations of values of α , β and ω at each Reynolds number for particular systems defined by the Rossby number and suction parameter. From these we form the dispersion relation, $D(\alpha, \beta, \omega; Re, Ro, a_s) = 0$, with the aim of studying the occurrence of convective and absolute instabilities at a particular location defined by Re . As previously discussed by Lingwood (see [14,2,27] for example), Briggs' [32] method will be used to distinguish between absolutely and convectively unstable time-asymptotic responses to the impulsive excitation of the boundary-layer flows in question. In what follows spatial branches (solutions lying in the complex α -plane for either real or complex ω) are calculated using a double-precision fixed-step-size, fourth-order Runge–Kutta integrator with Gram–Schmidt orthonormalisation and a Newton–Raphson linear search procedure, using the numerical code previously discussed by Lingwood.

3. Convective instability

We begin by supposing that the flow is not absolutely unstable, so that in Briggs' method we can reduce the imaginary part of the frequency to zero and proceed with a spatial convective analysis. We solve the eigenvalue problem defined by Eqs. (11)–(16) with the homogeneous boundary conditions (17) for $\alpha = \alpha_r + i\alpha_i$, and ω, β real.

3.1. Stationary modes

We begin by explicitly assuming that the disturbances rotate with the surface of the lower disk, which is consistent with

the experimental observations described in Section 1. The term *stationary* is used to denote disturbances that rotate with the surface of the lower disk, and *non-stationary* or *travelling* denotes those that have a relative azimuthal speed. In this frame of reference stationary disturbances are studied by enforcing $\omega = 0$.

In order to investigate the spatial branches for each parameter set $\{Ro, a_s\}$, we solve the dispersion relation for α while marching through values of β at fixed Re . In each case we find that two spatial branches determine the convective-instability characteristics of the system. These branches have been studied in depth for von Kármán and related flows (see [13,14,33,34], for example) and are typically labelled types I and II. The type I branch is known to arise from inviscid crossflow effects, originating from inflection points in the steady flow; and the type II branch is known to occur from a balance between viscous and Coriolis forces. The interaction of these branches at particular Reynolds numbers determines the neutral curves.

There exists a large number of possible parameter combinations and we present neutral curves at only a few of these. Critical Reynolds numbers for both mode types are given for a broader range of parameters in Table 1. Figs. 4 and 5 show neutral curves in terms of the wavenumber α for the convective instability of stationary modes. Fig. 4 demonstrates the interpretation of the results whereby a particular rotating system (defined by Ro) is subject to increased suction through the lower boundary. Fig. 5 displays the same neutral curves but grouped by fixed mass-flux parameter a_s . As discussed in Section 1, the von Kármán case ($Ro = -1$) has been studied by both Dhanak [24] and Lingwood [27] and is not presented here. The results for $Ro = 1$ extend those already presented by Culverhouse et al. [29]. Excellent agreement is found in cases where comparisons can be made.

We see that suction is universally stabilising, in the sense of increasing critical Reynolds numbers, with the exception of the Ekman case ($Ro = 0$) which is independent of the mass-flux parameter. Flows with large negative Ro are the most sensitive to mass flux, and this sensitivity is gradually reduced as Ro is increased towards the Ekman case. Beyond this the sensitivity again increases with positive Ro towards the Bödewadt case. As mentioned in Section 3.1, the radial and azimuthal flow components of the steady Ekman flow are independent of the mass-flux parameter, and we note that setting $Ro = 0$ removes all dependence on W within the stability Eqs. (11)–(16). We would therefore expect the stability properties of the Ekman layer to be independent of the mass flux, which is as found.

The neutral curves demonstrate that suction acts to increase the relative importance of the type II mode (lower lobe) to the type I mode (upper lobe). This is seen through either the appearance of the lower lobe with increased suction, or by making it more pronounced with respect to the type I lobe. Table 1 reflects this through the appearance of critical Reynolds numbers for the type II lobe on the right-hand side of the table only. The most dangerous stationary mode (in the sense of lowest critical Reynolds number) is plotted in Fig. 6. We see that for each $a_s \leq 0.8$ increasing Ro acts

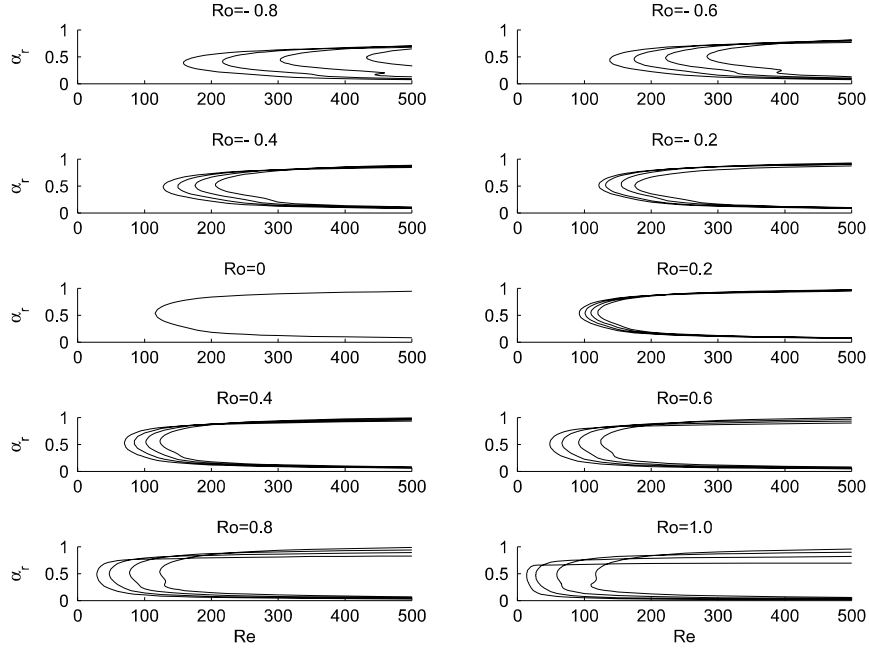


Fig. 4. Neutral curves for the convective instability of stationary modes at each Ro for $a_s = -0.4, 0, 0.4, 0.8$, left to right in each frame.

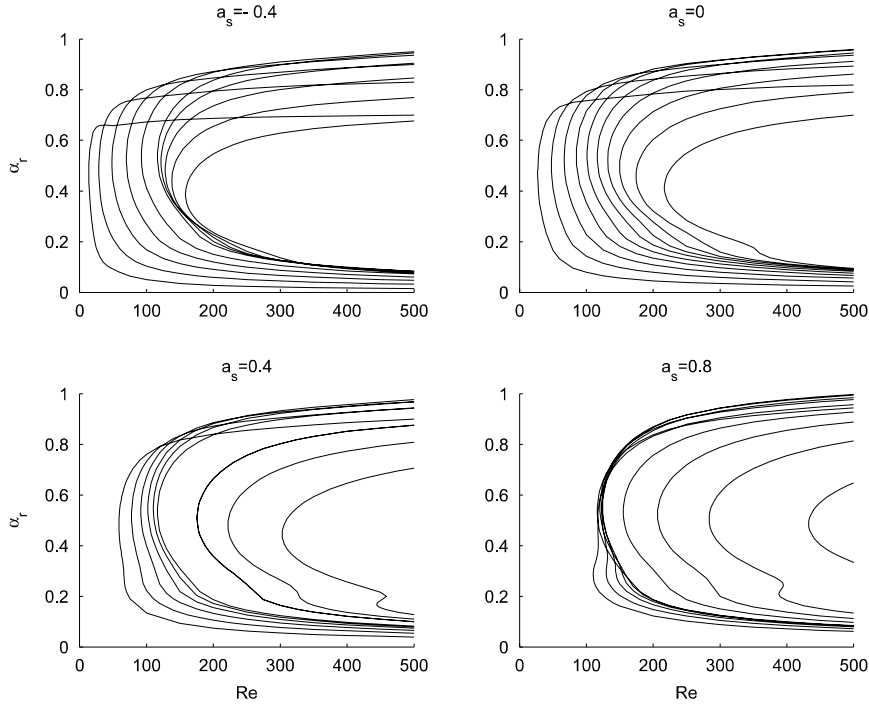


Fig. 5. Neutral curves for the convective instability of stationary modes at each a_s for $Ro = -0.8, \dots, 0.8, 1.0$, right to left in each frame.

to destabilise the boundary layer. Beyond this suction rate those flows characterised by positive Rossby number have the opposite behaviour. However, the results are such that increased suction is still stabilising for any particular Ro . Fig. 6 clearly demonstrates the particular sensitivity to suction of flows with large, negative Rossby number, as mentioned above.

Although little experimental data currently exists to compare our predictions with, we present computed values of experimentally measurable quantities in the Appendix. In particular the number, $|\bar{\beta}|$, and angle of orientation, $\epsilon = \arctan(\alpha/\beta)$, are given at the critical Reynolds numbers for the onset of each mode.

3.2. Travelling modes

Stationary waves are given particular attention because they are excited by unavoidable roughness on the surface of the lower disk, and, as mentioned in Section 1, are therefore often observed in experiments. However, waves travelling relative to the lower disk can be excited by freestream turbulence and have been observed experimentally in the von Kármán case by Fedorov [5], Lingwood [6] and Corke et al. [35], for example. Disturbances have dimensional frequency $\omega^* = \omega_r Re \Omega^*$, and so the quantity $\omega_s = \omega_r Re$ remains constant as disturbances propagate. We use

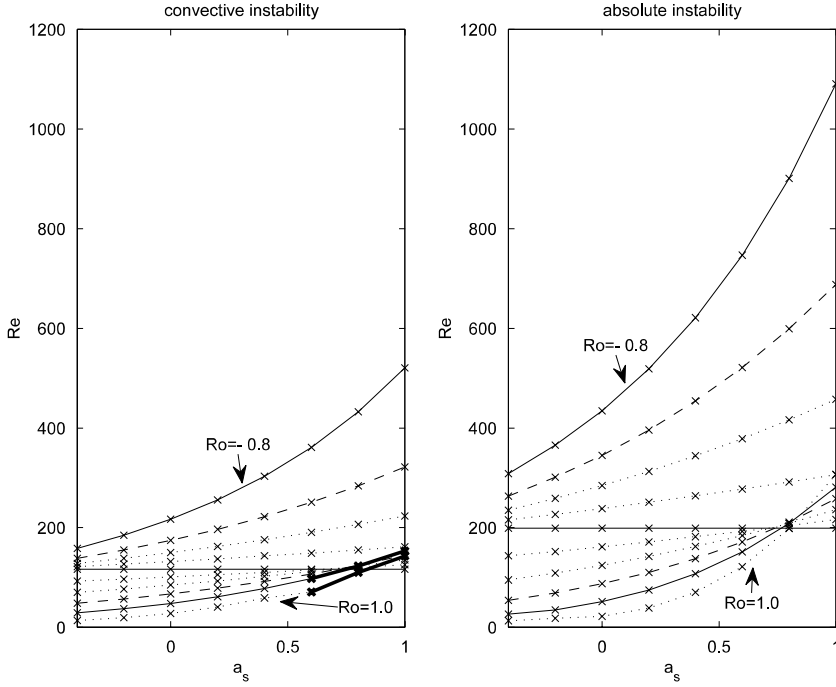


Fig. 6. Critical Reynolds numbers for the onset of the most dangerous stationary convective mode (the bold line indicates that type II is the most dangerous), and absolute instability. ($Ro = -0.8, -0.6, \dots, 1$ with $Ro = -0.8$ uppermost.)

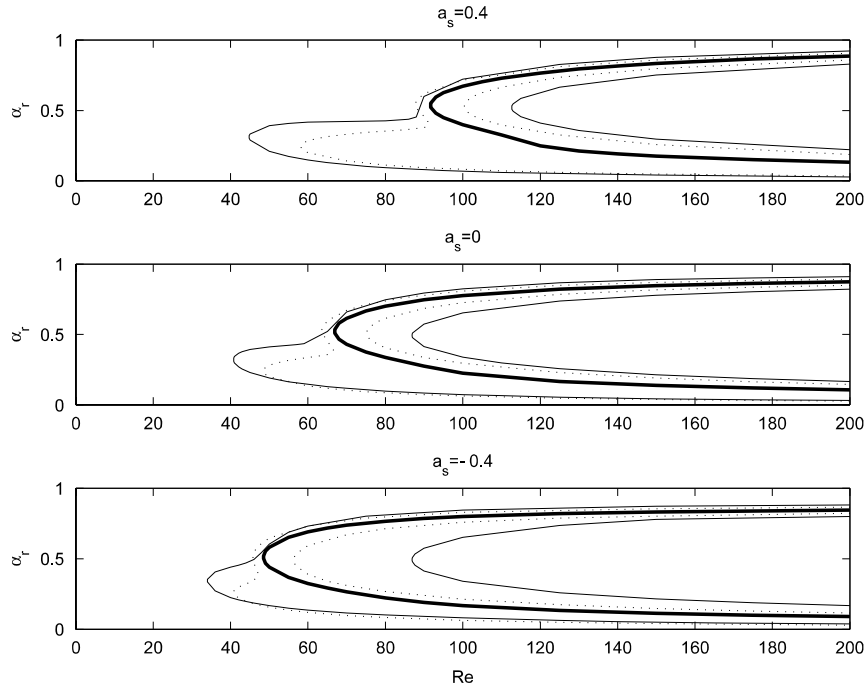


Fig. 7. Neutral curve for travelling convective modes at $Ro = 0.6$. Increasing $\omega_s = -10, -5, 0, 5, 10$ left to right (the bold line indicates the stationary mode).

non-zero ω_s to enforce travelling waves within our theoretical system. Disturbances with $\omega_s > 0$ represent waves with positive azimuthal phase-velocity component in the rotating frame and are considered to be rotating more quickly than the lower disk surface; waves with $\omega_s < 0$ represent waves with negative azimuthal phase-velocity component and are considered to be rotating more slowly. Introducing this additional parameter increases the number of possible cases to be studied and we are forced to limit our investigation. Furthermore, as we will see in Section 4,

each flow becomes absolutely unstable beyond a particular critical Reynolds number as determined by the behaviour of the type I branch at a particular ω_s .

Fig. 7 shows neutral curves for travelling modes at $Ro = 0.6$. We find that slowly travelling type II modes can be significantly more dangerous (in the sense of lower critical Reynolds numbers) than the type I mode which dominates for stationary waves. This behaviour occurs at each a_s considered but is less significant with increased suction. In each case the critical Reynolds numbers of the

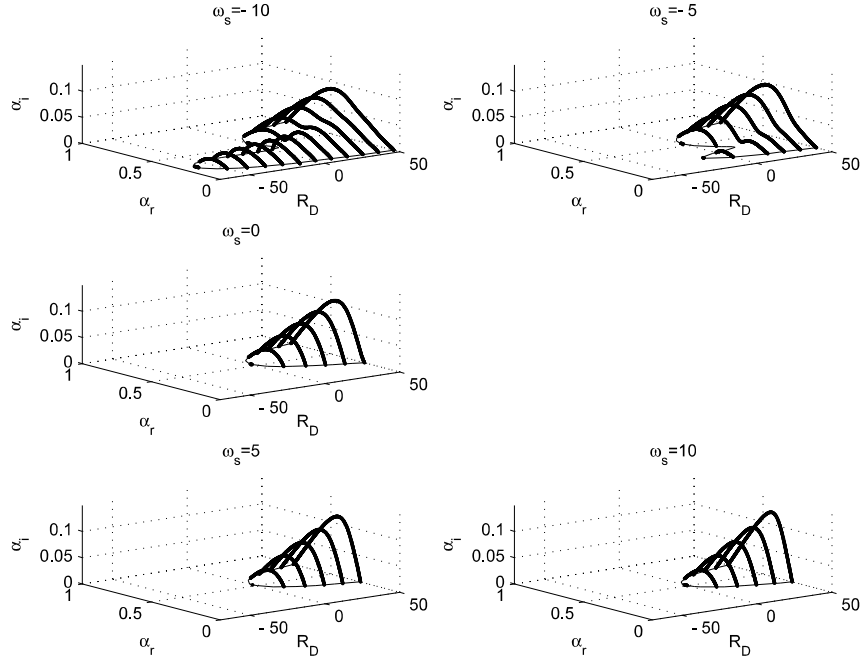


Fig. 8. Linear convective growth rates for travelling mode disturbances at $Ro = 0$.

type I mode is only marginally reduced with reduced ω_s . Similar behaviour is observed at all other Ro and we do not show further neutral curves here.

It is also possible to study the linear amplification rates of the unstable spatial modes, $|\alpha_i|$, within the convectively unstable region of each flow. We introduce the quantity $R_D = Re - Re_{\text{crit}}$, the distance into the unstable region from the onset of the type I convective mode at each particular ω_s , and plot $|\alpha_i|$ against $R_D < 50$. Fig. 8 demonstrates convective growth rates of travelling modes at $Ro = 0$. With regard to the type I mode, we see that modes with positive ω_s have marginally greater growth rates. However, given these small changes in growth rate, we would expect the effect of delayed onset to dominate. Growth rates of the type I mode reduce for slowly travelling waves with decreased ω_s , however, the type II mode growth rates increase in addition to having significantly lower critical Reynolds numbers. This behaviour has been found at all Ro tested. We therefore expect travelling type II modes to play a significant role in the convective regimes for all flows within the BEK classification, dependent on receptivity mechanisms, especially for highly polished disks where the effects of roughness are minimised and stationary disturbances are linear.

Although not shown here, the growth rates of travelling type I and type II modes are significantly affected by mass flux. As would be expected, increased suction decreases amplification rates for all flows within the BEK system and is stabilising in this sense too. For example, for $Ro = 0.6$ and $\omega_s = 5$, the maximum amplification rate for $a_s = 0.4$ is around 60% of that with zero mass flux at any R_D . In contrast, for $a_s = -0.4$, the maximum amplification rate is around 170% of that with zero mass flux at the same R_D . Similar behaviour is found for other Ro and ω_s .

4. Absolute instability

Absolute instability can be identified by singularities in the dispersion relation that occur when waves that propagate energy in different directions coalesce. It is known that variation of the Reynolds number, for example, of a particular system can cause pinch-points to occur, leading to the flow changing from the

convectively unstable to the absolutely unstable regime. A spatio-temporal analysis is necessarily required in this part of the study and we must consider α and ω as complex quantities, while β remains real to enforce periodicity round the azimuth. The term spatial branch is used in this context but here it refers to solutions of the dispersion relation that lie in the α -plane and have complex ω .

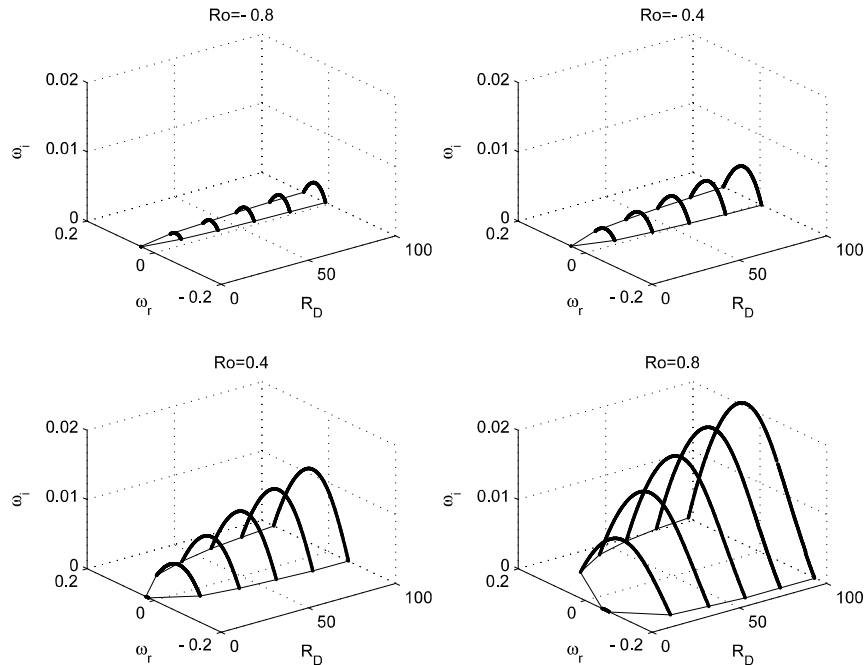
We apply Briggs' criterion with fixed β to distinguish between convectively and absolutely unstable time-asymptotic responses to an initial boundary-value perturbation. The perturbation is provided by an impulsive line forcing at time $t = 0$ (see Lingwood [36]). The criterion for absolute instability requires branch-point singularities between at least two spatial branches of the dispersion relation. In order for the singularity to be a pinch-point, two of these branches must lie in distinct half α -planes when ω_i is sufficiently large and positive. If $\omega_i > 0$ at the pinch-point the flow is absolutely unstable, otherwise the flow is only convectively unstable or stable. Practical use of this method has been discussed in detail by Lingwood [14,2], amongst others, and the interested reader is referred there.

Pinch-points with $\omega_i > 0$ have been found for all parameter sets $\{Ro, a_s\}$, and so all boundary-layer flows within the BEK system are absolutely unstable for certain values of Re and β . Lingwood [2] discusses the absolute instability properties of the flows with zero mass flux; in particular she mentions that the upper branch of the neutral curves for $0.8 \leq Ro \leq 1$ is discontinuous because the branch points cease being pinch-points for sufficiently high Reynolds numbers. We also find this to be true for non-zero mass flux, although the feature is not physically relevant because absolute instability at lower Reynolds number would already have promoted the onset of non-linearity and possibly laminar-turbulent transition.

Lingwood [27] considers the effects of imposed mass flux for the von Kármán boundary layer and this case is not considered here. At general Ro , all neutral curves are qualitatively similar to those previously presented by Lingwood [14,2,27] and are not presented here. Instead we state the critical Reynolds numbers for the onset of absolute instability in Table 2. This data is plotted in Fig. 6 where we see that increasing Ro acts to destabilise (lower critical Reynolds number) the boundary layer to absolute instabilities at

Table 2Critical Reynolds numbers Re at the onset of absolute instability.

Ro	$a_s = -0.4$	$a_s = -0.2$	$a_s = 0$	$a_s = 0.2$	$a_s = 0.4$	$a_s = 0.6$	$a_s = 0.8$	$a_s = 1.0$
-0.8	308.4	365.4	434.4	518.5	621.2	746.9	901.0	1090.6
-0.6	263.0	301.2	345.1	395.9	454.3	521.5	598.9	687.8
-0.4	234.9	258.5	284.5	313.1	344.4	378.7	416.4	457.6
-0.2	215.3	226.5	238.3	250.7	263.7	277.3	291.5	306.5
0	198.8	198.8	198.8	198.8	198.8	198.8	198.8	198.8
0.2	143.3	152.1	161.4	171.3	181.7	192.7	204.2	216.3
0.4	95.1	108.9	124.6	142.2	162	184.2	208.9	236.3
0.6	54.5	69.1	87.4	110.1	137.8	171.2	211.1	258.1
0.8	26.4	34.6	51.5	74.9	107.5	151.4	208.5	281.5
1	13.2	18.1	21.7	38.6	70.3	121.5	198.3	307

**Fig. 9.** Absolute growth rates through a fixed distance into the absolutely unstable region.

each $a_s \leq 0.8$; beyond this suction rate those flows characterised by positive Rossby number have the opposite behaviour. However we note that suction is universally stabilising for any particular Ro (results for $Ro = 0$ are independent of mass flux). Flows with large negative Rossby number show particular sensitivity to non-zero mass flux. The response of absolute instability to mass flux is therefore very similar to that found for convective instabilities in Section 3.1. Further information on the critical parameters is given in the Appendix. Where applicable this data shows agreement with related studies.

It is possible to consider growth rates through the absolutely unstable region, ω_i . Similarly to the convective instability study, we define R_D to be the Reynolds-number distance into the absolutely unstable region and plot ω_i for $R_D < 100$. Fig. 9 compares the absolute growth rates through this region across Ro for $a_s = 0$. We find that the growth rates increase significantly with increased Ro . This general behaviour was found at all a_s .

Although not shown here, it was also found that increased suction acts to reduce the maximum growth rates at each particular Ro . This is consistent with the notion that suction is a stabilising mechanism to absolute instability. For example, at $Ro = 0.8$, the maximum amplification rate for $a_s = 0.4$ is around 40% of that with zero mass flux at any particular R_D . In contrast, for $a_s = -0.4$, the maximum amplification rate is around 400% of that with zero mass flux at the same R_D . Similar behaviour is found for other Ro .

5. Conclusion

In this study we have demonstrated that each flow defined by the parameter set $\{Ro, a_s\}$ within the BEK system exhibits laminar flow at radial positions close to the axis of rotation, and regions of convective and absolute instability at larger radial positions. As mentioned in Section 2.1, the sign of the Rossby number has implications for the direction of wave propagation within the unstable regimes and this needs careful consideration. For $Ro < 0$ the radial mean flow is directed predominantly outwards and convective modes propagate outwards. In contrast, for $Ro \geq 0$ the radial mean flow is directed predominantly inwards and convective modes propagate inwards.

For $Ro \leq 0$ and at all a_s , the convectively unstable regime is found at lower radial positions than the absolutely unstable regime (see Tables 1 and 2). This is as required from the type I branch crossing the α_r -axis prior to pinching and the onset of absolute instability. Convectively unstable modes then propagate outwards towards the region of absolute instability leading to transition. However, for $Ro > 0$ the situation is more complicated. Again the convectively unstable region exists at lower radii than the absolutely unstable region for all flows.²

² Although, in contrast to $Ro \leq 0$, this is not clear from Tables 1 and 2 as one has to consider the more dangerous travelling convective modes.

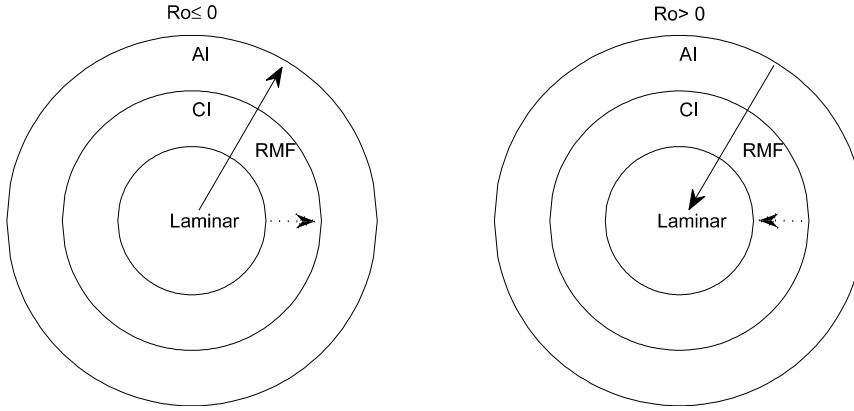


Fig. 10. Sketch of the lower rotating disk, indicating the regions of laminar flow, convective instability (CI) and absolute instability (AI). Arrows demonstrate the direction of the net radial mean flow (RMF) and propagation of the convectively unstable modes involved in the absolutely instability (dotted arrows).

Table A.3

Critical values of α at the onset of stationary type I lobes. Where appropriate the critical value at the onset of the stationary type II lobe is also shown, (*italics*).

Ro	$a_s = -0.4$	$a_s = -0.2$	$a_s = 0$	$a_s = 0.2$	$a_s = 0.4$	$a_s = 0.6$	$a_s = 0.8$	$a_s = 1.0$
-0.8	0.387	0.400	0.413	0.428 (0.165)	0.445 (0.171)	0.464 (0.175)	0.489 (0.182)	0.508 (0.193)
-0.6	0.440	0.448	0.459	0.469	0.481	0.493 (0.209)	0.506 (0.209)	0.520 (0.213)
-0.4	0.483	0.489	0.495	0.502	0.509	0.516	0.524	0.531
-0.2	0.515	0.518	0.521	0.524	0.528	0.531	0.534	0.537
0	0.536	0.536	0.536	0.536	0.536	0.536	0.536	0.536
0.2	0.536	0.538	0.541	0.544	0.547	0.550	0.552	0.555
0.4	0.528	0.532	0.537	0.542	0.548	0.552	0.558	0.565
0.6	0.510	0.517	0.523	0.530	0.537	0.545	0.553	0.562
0.8	0.485	0.493	0.500	0.508	0.516	0.525	0.535	0.546
1	0.472	0.474	0.469	0.476	0.483	0.486 (0.280)	0.490 (0.288)	(0.295)

Table A.4

Number of vortices, $n = \beta R$, at the onset of stationary type I lobes. Where appropriate the critical value at the onset of the stationary type II lobe is also shown, (*italics*).

Ro	$a_s = -0.4$	$a_s = -0.2$	$a_s = 0$	$a_s = 0.2$	$a_s = 0.4$	$a_s = 0.6$	$a_s = 0.8$	$a_s = 1.0$
-0.8	15.97	18.30	20.96	24.05 (23.81)	27.51 (25.80)	31.85 (27.65)	36.71 (30.1)	42.26 (32.95)
-0.6	15.98	17.62	19.60	21.75	24.18	26.82 (25.69)	29.76 (27.12)	33.00 (28.77)
-0.4	16.10	17.31	18.62	20.03	21.49	23.08	24.80	26.55
-0.2	16.25	16.86	17.52	18.16	18.87	19.58	20.30	21.07
0	16.04	16.04	16.04	16.04	16.04	16.04	16.04	16.04
0.2	13.00	13.56	14.16	14.77	15.39	16.06	16.72	17.42
0.4	9.78	10.77	11.91	12.99	14.23	15.53	16.95	18.47
0.6	6.51	7.74	9.13	10.70	12.46	14.42	16.60	19.00
0.8	3.45	4.65	6.14	7.97	10.10	12.60	15.50	18.79
1	1.11	2.00	3.14	4.86	7.16	8.52 (7.96)	13.40 (10.65)	(12.83)

Table A.5

Orientation angle ϵ at the onset of stationary type I lobes. Where appropriate the critical value at the onset of the stationary type II lobe is also shown, (*italics*).

Ro	$a_s = -0.4$	$a_s = -0.2$	$a_s = 0$	$a_s = 0.2$	$a_s = 0.4$	$a_s = 0.6$	$a_s = 0.8$	$a_s = 1.0$
-0.8	14.6	13.9	13.2	12.4 (19.8)	11.6 (18.7)	10.8 (17.6)	9.9 (16.3)	9.1 (14.9)
-0.6	15.2	14.5	14.2	13.7	13.1	12.5 (18.7)	11.7 (18.5)	11.2 (17.7)
-0.4	14.6	14.3	14.1	13.8	13.5	13.2	12.9	12.6
-0.2	14.5	14.4	14.3	14.2	14.0	13.9	13.8	13.7
0	14.4	14.4	14.4	14.4	14.4	14.4	14.4	14.4
0.2	14.7	14.6	14.5	14.4	14.3	14.2	14.1	14.0
0.4	14.8	14.7	14.6	14.4	14.3	14.1	13.8	13.6
0.6	14.7	14.7	14.6	14.5	14.2	13.9	13.6	13.2
0.8	13.9	14.3	14.5	14.4	14.2	13.8	13.2	12.7
1	9.7	12.4	13.7	14.2	14.1	14.0 (20.7)	13.1 (18.6)	(12.8)

However, disturbance waves from the convective regime would then propagate inwards towards the stable regime, decaying as they do so. Disturbances originating in the absolutely unstable regime would grow quickly, promoting non-linearity and the onset to turbulence before the convectively unstable regime is reached. The transition mechanism is expected to result in a similar situation to the negative-Rossby-number flows whereby a flow

structure qualitatively similar to transition with the von Kármán boundary layer would occur. This is summarised in Fig. 10.

Low critical Reynolds numbers have been computed for the onset of both instability types for Ro approaching unity, and we would expect that the flows are extremely unstable with turbulence occurring close to the axis of rotation. However, this is inconsistent with experimental observations of the Bödewadt layer

Table A.6Critical values of α at the onset of absolute instability.

Ro	$a_s = -0.4$	$a_s = -0.2$	$a_s = 0$	$a_s = 0.2$	$a_s = 0.4$	$a_s = 0.6$	$a_s = 0.8$	$a_s = 1.0$
-0.8	-0.238-i0.138	-0.244-i0.140	-0.252-i0.142	-0.260-i0.145	-0.270-i0.147	-0.281-i0.149	-0.292-i0.152	-0.308-i0.155
-0.6	-0.286-i0.159	-0.290-i0.162	-0.294-i0.164	-0.299-i0.166	-0.304-i0.169	-0.310-i0.171	-0.316-i0.173	-0.324-i0.176
-0.4	-0.326-i0.176	-0.327-i0.178	-0.329-i0.180	-0.331-i0.182	-0.333-i0.184	-0.337-i0.186	-0.340-i0.188	-0.343-i0.189
-0.2	-0.356-i0.188	-0.356-i0.189	-0.357-i0.190	-0.358-i0.192	-0.358-i0.193	-0.359-i0.194	-0.360-i0.195	-0.361-i0.196
0	0.378+i0.196							
0.2	0.394+i0.193	0.394+i0.195	0.393+i0.196	0.393+i0.198	0.392+i0.200	0.392+i0.202	0.392+i0.203	0.392+i0.205
0.4	0.409+i0.179	0.406+i0.184	0.403+i0.191	0.402+i0.196	0.400+i0.200	0.399+i0.204	0.399+i0.207	0.399+i0.211
0.6	0.420+i0.145	0.415+i0.163	0.410+i0.176	0.405+i0.187	0.401+i0.195	0.399+i0.202	0.398+i0.208	0.399+i0.213
0.8	0.490-i0.046	0.378+i0.115	0.407+i0.141	0.403+i0.167	0.397+i0.185	0.392+i0.197	0.390+i0.205	0.391+i0.212
1	0.491-i0.032	0.498-i0.026	0.341+i0.079	0.366+i0.125	0.385+i0.162	0.378+i0.186	0.375+i0.199	0.376+i0.207

Table A.7Critical values of β at the onset of absolute instability.

Ro	$a_s = -0.4$	$a_s = -0.2$	$a_s = 0$	$a_s = 0.2$	$a_s = 0.4$	$a_s = 0.6$	$a_s = 0.8$	$a_s = 1.0$
-0.8	0.158	0.156	0.155	0.152	0.149	0.146	0.142	0.137
-0.6	0.170	0.170	0.169	0.168	0.167	0.165	0.164	0.161
-0.4	0.177	0.178	0.178	0.179	0.179	0.179	0.178	0.178
-0.2	0.181	0.182	0.183	0.183	0.184	0.184	0.185	0.185
0	0.181	0.181	0.181	0.181	0.181	0.181	0.181	0.181
0.2	0.169	0.171	0.174	0.176	0.178	0.180	0.181	0.182
0.4	0.139	0.152	0.158	0.164	0.170	0.175	0.178	0.181
0.6	0.067	0.101	0.126	0.144	0.157	0.166	0.173	0.177
0.8	-0.113	-0.049	0.051	0.104	0.135	0.154	0.164	0.169
1	-0.104	-0.079	-0.115	-0.008	0.0919	0.134	0.152	0.157

Table A.8Critical values of ω at the onset of absolute instability.

Ro	$a_s = -0.4$	$a_s = -0.2$	$a_s = 0$	$a_s = 0.2$	$a_s = 0.4$	$a_s = 0.6$	$a_s = 0.8$	$a_s = 1.0$
-0.8	0.0400	0.0396	0.0391	0.0385	0.0378	0.0370	0.0360	0.0343
-0.6	0.0415	0.0416	0.0417	0.0418	0.0416	0.0414	0.0410	0.0406
-0.4	0.0414	0.0420	0.0426	0.0430	0.0434	0.0437	0.0438	0.0439
-0.2	0.0402	0.0408	0.0415	0.0420	0.0425	0.0430	0.0434	0.0437
0	0.0381	0.0381	0.0381	0.0381	0.0381	0.0381	0.0381	0.0381
0.2	0.0280	0.0299	0.0316	0.0333	0.0348	0.0362	0.0374	0.0386
0.4	0.0062	0.0156	0.0203	0.0256	0.0301	0.0337	0.0368	0.0393
0.6	-0.0508	-0.0223	-0.0022	0.0123	0.02290	0.03044	0.03589	0.0397
0.8	-0.2168	-0.1502	-0.0608	-0.0154	0.0105	0.0256	0.0345	0.03955
1	-0.1919	-0.1771	-0.2155	-0.1070	-0.0181	0.0175	0.0326	0.0386

Table A.9Critical values of ω_s at the onset of absolute instability.

Ro	$a_s = -0.4$	$a_s = -0.2$	$a_s = 0$	$a_s = 0.2$	$a_s = 0.4$	$a_s = 0.6$	$a_s = 0.8$	$a_s = 1.0$
-0.8	12.3	14.5	17.0	20.0	23.5	27.6	32.4	37.4
-0.6	10.9	12.5	14.4	16.5	18.9	21.6	24.6	27.9
-0.4	9.7	10.9	12.1	13.5	14.9	16.5	18.2	20.1
-0.2	8.7	9.2	9.9	10.5	11.2	11.9	12.7	13.4
0	7.6	7.6	7.6	7.6	7.6	7.6	7.6	7.6
0.2	4.0	4.5	5.1	5.7	6.3	7.0	7.6	8.3
0.4	0.6	1.7	2.5	3.6	4.9	6.2	7.7	9.3
0.6	-2.8	-1.5	-0.2	1.4	3.2	5.2	7.6	10.2
0.8	-5.7	-5.2	-3.1	-1.2	1.1	3.9	7.2	11.1
1	-2.5	-3.2	-4.7	-4.1	-1.3	2.1	6.5	11.9

[8–12] which report a substantial region within which convectively unstable waves exist. Furthermore, Culverhouse et al. [29] neglect the onset of absolute instability and detail asymptotic and numerical studies of the convectively unstable region of this flow and find good agreement with the experimental results of Cros et al. [12]. In response to this inconsistency, we note that the parallel-flow approximation made throughout our study would be significant for flows with such low Reynolds numbers. Our results for absolute instability are therefore of questionable validity as Ro tends to unity.

We find that increased suction acts to extend significantly the radial span of the convectively unstable region at all Rossby numbers. The sensitivity to this is seen to be greatest for large,

negative Ro , but increases as Ro tends to either ± 1 . For systems with fixed Ro , we predict suction to be a stabilising mechanism in the sense of delaying both the onset of transition and turbulence and also increasing the size of the convectively unstable region before absolute instability is reached. Suction is also seen to reduce the growth rates of all instability modes.

Interpreting the results in terms of fixed mass flux but varying Rossby number, we find that increasing Ro acts to destabilise the boundary layer to both convective and absolute instabilities at each $a_s \leq 0.8$; beyond this suction rate those flows characterised by positive Rossby number demonstrate the opposite behaviour.

Within the convectively unstable region, type II modes with negative ω_s are predicted to be the most dangerous in terms of

both onset and amplification rate. In practical cases where surface roughness is unavoidable, stationary modes are still expected to be excited.

Appendix. Critical values of measurable quantities

A.1. Convective instability

See Tables A.3–A.5.

A.2. Absolute instability

See Tables A.6–A.9.

References

- [1] N. Gregory, J.T. Stuart, W.S. Walker, On the stability of three-dimensional boundary layers with application to the flow due to a rotating disk, *Philos. Trans. R. Soc. Lond. Ser. A* 248 (1955) 155–199.
- [2] R.J. Lingwood, Absolute instability of the Ekman layer and related rotating flows, *J. Fluid Mech.* 331 (1997) 405–428.
- [3] P.R. Tattro, E.L. Mollö-Christensen, Experiments on Ekman layer instability, *J. Fluid Mech.* 28 (1967) 531–543.
- [4] A.J. Faller, An experimental study of the instability of the Ekman boundary layer, *J. Fluid Mech.* 15 (1963) 560–576.
- [5] B.I. Fedorov, G.Z. Plavnik, I.V. Prokhorov, L.G. Zhukhovitskii, Transition conditions on a rotating disc, *J. Eng. Phys.* 31 (1976) 1060–1067.
- [6] R.J. Lingwood, An experimental study of absolute instability of the rotating-disk boundary-layer flow, *J. Fluid Mech.* 314 (1996) 373–405.
- [7] T.C. Corke, K.F. Knasiak, Stationary travelling cross-flow mode interactions on a rotating disk, *J. Fluid Mech.* 355 (1998) 285–315.
- [8] Ö. Savaş, Stability of Bödewadt flow, *J. Fluid Mech.* 183 (1987) 77–94.
- [9] J.M. Lopez, Flow between a stationary and rotating disk shrouded by a co-rotating cylinder, *Phys. Fluids* 8 (1996) 2605–2613.
- [10] R.J. Lingwood, P.H. Alfredsson, Experimental study of the stability of the Bödewadt layer, in: Proceedings of the IUTAM Symposium, Sedona, Arizona, vol. 24, 1999, pp. 409–424.
- [11] L. Schouveiler, P. Le Gal, M.P. Chauve, Instabilities of the flow between a rotating and a stationary disk, *J. Fluid Mech.* 443 (2001) 329–350.
- [12] A. Cros, E. Floriani, P. Le Gal, R. Lima, Transition to turbulence of the Batchelor flow in a rotor/stator device, *Eur. J. Mech. B Fluids* 24 (2005) 409–424.
- [13] M.R. Malik, The neutral curve for stationary disturbances in rotating-disk flow, *J. Fluid Mech.* 164 (1986) 275–287.
- [14] R.J. Lingwood, Absolute instability of the boundary layer on a rotating disk, *J. Fluid Mech.* 299 (1995) 17–33.
- [15] N. Itoh, Structure of absolute instability in 3-D boundary layers; part 1. Mathematical formulation, *Trans. Japan Soc. Aeronaut. Space Sci.* 44 (144) (2001) 96–100.
- [16] N. Itoh, Structure of absolute instability in 3-D boundary layers; part 2. Application to rotating-disk flow, *Trans. Japan Soc. Aeronaut. Space Sci.* 44 (144) (2001) 101–105.
- [17] C. Davies, P.W. Carpenter, 'Global behaviour corresponding to the absolute instability of the rotating-disk' boundary layer, *J. Fluid Mech.* 486 (2003) 287–329.
- [18] S.J. Garrett, N. Peake, On the global linear stability of the boundary layer on rotating bodies, in: J.M.L.M. Palma, & A. Silva Lopes, (Eds.), *Advances in Turbulence XI: Proceedings of the 11th EUROMECH European Turbulence Conference*, 2007, pp. 550–552.
- [19] B. Pier, Finite-amplitude crossflow vortices, secondary instability and transition in the rotating-disk boundary layer, *J. Fluid Mech.* 487 (2003) 315–343.
- [20] N. Gregory, W.S. Walker, Experiments on the effect of suction on the flow due to a rotating disk, *Philos. Trans. R. Soc. Lond.* 248 (1960) 225–234.
- [21] N. Gregory, W.S. Walker, Experiments on the effect of suction on the flow due to a rotating disk, *Rep. Aero. Res. Coun. Lond.* 16 (1953) 152.
- [22] J.T. Stuart, On the effect of uniform suction on the steady flow due to a rotating disk, *Quart. J. Mech. Appl. Math.* 7 (1954) 446–457.
- [23] H. Ockendon, An asymptotic solution for steady flow above an infinite rotating disc with suction, *Quart. J. Mech. Appl. Math.* 25 (1971) 291–301.
- [24] M.R. Dhanak, Effects of uniform suction on the stability of flow on a rotating disk, *Proc. R. Soc. Lond. Ser. A* 439 (1992) 431–440.
- [25] A.P. Bassom, S.O. Seddougui, The effects of suction on the nonlinear stability of the three-dimensional boundary layer above a rotating disk, *Proc. R. Soc. Lond. Ser. A* 436 (1992) 405–415.
- [26] M. Turkyilmazoglu, Lower branch modes of the compressible boundary layer due to a rotating-disk, *Stud. Appl. Math.* 114 (2005) 17–43.
- [27] R.J. Lingwood, On the effects of suction and injection on the absolute instability of a rotating-disk boundary layer, *Phys. Fluids* 9 (1997) 13–17.
- [28] T. von Kármán, Über laminare und turbulente Reibung, *ZAMM Z. Angew. Math. Mech.* 1 (1921) 233–252.
- [29] N.A. Culverhouse, S.J. Garrett, S.O. Stephen, R.J. Lingwood, The effects of mass flux on travelling modes within the Bödewadt layer (2011) (submitted for publication).
- [30] A.I. van de Vooren, E.F.F. Botta, J. Stout, The boundary layer on a disc at rest in a rotating fluid, *Quart. J. Mech. Appl. Math.* 40 (1987) 15–32.
- [31] S.O. MacKerrell, Stability of Bödewadt flow, *Philos. Trans. R. Soc. Lond. Ser. A* 363 (2005) 1181–1187.
- [32] R.J. Briggs, *Electron-Stream Interaction with Plasmas*, MIT Press, 1964.
- [33] S.J. Garrett, N. Peake, The stability and transition of the boundary layer on a rotating sphere, *J. Fluid Mech.* 456 (2002) 199–218.
- [34] S.J. Garrett, Z. Hussain, S.O. Stephen, The crossflow instability of the boundary layer on a rotating cone, *J. Fluid Mech.* 622 (2009) 209–232.
- [35] T.C. Corke, E.H. Matlis, H. Othman, Transition to turbulence in rotating-disk boundary layers - convective and absolute instabilities, *J. Eng. Math.* 57 (2007) 253–272.
- [36] R.J. Lingwood, On the application of the Briggs' and steepest-descent methods to a boundary-layer flow, *Stud. Appl. Math.* 98 (2007) 213–254.